A HIGH-RESOLUTION H I STUDY OF THE INTERSTELLAR MEDIUM LOCAL TO HD 193793

E. MARCELO ARNAL[1,2]

Facultad de Ciencias Astronómicas y Geofísicas, Paseo del Bosque s/n, 1900 La Plata, Argentina; and Instituto Argentino de Radioastronomía,
C.C. No. 5, 1894 Villa Elisa, Argentina

ABSTRACT

A 2° field centered at the optical position of the Wolf-Rayet (WR) star HD 193793 ($\equiv$ WR 140) was surveyed in the H I 21 cm line and in the 1420 MHz radio continuum, using the Dominion Radio Astrophysical Observatory interferometer. The aim of this observations was to look for evidence of an interaction between the WR star and its local interstellar medium (ISM). Our H I data displays a large oval minimum at a velocity of $V_{sys} \simeq -12$ km s^{-1}, close to the optical position of HD 193793. We believe this H I void was created by WR 140 and its massive companion (HD 193793 is a member of a well-known binary system). The major axis of the H I void is ~ 11.5 pc and its axial ratio, the ratio of major to minor axis, is ~ 1.4. This structure is observable over a velocity range of around 11 km s^{-1}. The H I minimum appears surrounded by a clumpy shell of H I in emission that has a total mass of neutral hydrogen of $M_{H I} \sim 1300$ solar masses. The kinematical distance corresponding to a local standard of rest velocity of -12 km s^{-1} is approximately 5.4 kpc, which disagrees with the distance of HD 193793, namely, around 1 kpc. Therefore, it is concluded that the H I bubble was blown in an ISM having nonnegligible peculiar motions. *Hipparcos* proper-motion measurements indicate that HD 193793 has a tangential velocity of 28 ± 3 km s^{-1} *along* the major axis of one of the H I minima detected in the interior of the main H I cavity. To reconcile this motion with the physical size of the H I structure blown by the winds of the binary system, it is concluded that such tangential velocity was acquired by the system a short while ago, namely, $\sim 1.3 \times 10^5$ yr. Maps from the *IRAS* database show a large-scale IR feature, with good spatial correlation with the H I shell surrounding the main H I void. We believe the emission from the IR shell arises from dust grains heated by the energetic stellar continuum photons emitted by the stellar objects.

Key words: ISM: bubbles — radio emission lines — stars: individual (HD 193793) — stars: Wolf-Rayet

1. INTRODUCTION

This is the second in a series of papers dealing with aperture synthesis observations of $\lambda \sim 21$ cm H I in the direction of Galactic Wolf-Rayet (WR) stars, using the 0.6 km array of the Dominion Radio Astrophysical Observatory (DRAO; Roger et al. 1973; Veidt et al. 1985). In a previous paper of this series, Arnal & Roger 1997, (hereafter referred to as Paper I), the interstellar medium local to the Galactic WR star HD 9974 was analyzed. The main finding was the presence of an ovoid H I minimum having an inner dual-minimum geometry. We believed this morphology was created by the joint action of the stellar winds of the WR star and its progenitor. A similar finding was also reported for WR 6 ($\equiv$ HD 50896) by Arnal & Cappa (1996).

In this paper we report on high-resolution H I 21 cm line observations, carried out toward the Galactic WR star WR 140 ($\equiv$ HD 193793). Based on intermediate (HPBW $\simeq 9'$) angular resolution data, it was found that WR 140 is related to a region showing a low neutral hydrogen emissivity (Arnal 1992). WR 140 is a long-period (~ 7.9 yr) binary with a highly eccentric orbit ($e \simeq 0.84$) (Williams et al. 1990). The WR star is classified as a WC7 (van der Hucht et al. 1988; Smith, Shara, & Moffat 1990), and its companion star is a O4–5 star (Lamontagne, Moffat, & Seggewiss 1984). The wind terminal velocity and the mass-loss rate of the Wolf-

Rayet star are 2800 km s^{-1} and $(6.0–6.3) \times 10^{-5} M_\odot$ yr^{-1} (Nugis, Crowther, & Willis 1998), respectively. Large and variable nonthermal radio emission has been detected from this binary system. It has been demonstrated by Williams et al. (1990) and van der Hucht (1992) that the nonthermal radio emission is associated with the colliding WR and O stellar winds, and that the variability is caused by optical depth effects due to phase-dependent orbital modulation. This system has been thoroughly observed at several wavelength ranges. A model to interpret the radio variability of this system has been presented by Becker & White (1985), based on an eight-year VLA monitoring of the HD 193793 radio flux at 2, 6, and 20 cm, respectively. At X-ray wavelengths a variable flux about an order of magnitude higher than that expected for WR stars has been observed (van der Hucht 1992). Recently, *Advanced Satellite for Cosmology and Astrophysics* (*ASCA*) observations of this system have also been reported (Skinner et al. 1995). Dust formation episodes in this system are also known to have taken place (Williams et al. 1987). Various distance determinations for this binary system exist, namely 0.8 kpc (Conti & Vacca 1990), 1.01 kpc (Hidayat, Supelli, & van der Hucht 1982), 1.21 kpc (Nugis et al. 1998), 1.34 kpc (van der Hucht et al. 1988), and 1.32 kpc (Smith et al. 1990).

A large *IRAS* shell centered at the optical position of WR 140, having an angular diameter of $110'$ and a dust mass of $710 M_\odot$, was reported by Marston (1996).

2. OBSERVATION AND DATA REDUCTION

Aimed at studying in detail the small-scale structure of the interstellar medium (ISM) around WR 140 and its

---

[1] Member of the Carrera del Investigador Científico, CONICET, Argentina.
[2] Visiting Astronomer, Dominion Radio Astrophysical Observatory, Penticton, British Columbia, Canada.

massive binary companion, a 2° field centered at the optical position of the WR star was studied using the DRAO aperture synthesis telescope (ST). The large field of view, high angular resolution, and reasonable sensitivity for mapping extended structures make this instrument ideally suited for studies of this kind. The observational parameters are summarized in Table 1.

The 21 cm H I spectral line was detected separately in right and left circular polarizations in two 128-channel digital correlation spectrometers for baselines from 13 to 600 m. The limited number of spectrometer channels were distributed in this way to maximize sensitivity at the expense of higher resolution. Simultaneously, the 21 cm continuum emission for both polarizations in two continuum bands placed on each side of the Galactic line emission were separately observed for all baselines up to 600 m. In addition, 74 cm (408 MHz) continuum emission was also simultaneously observed, but it is not considered any further in this study because of contamination by the nearby strong source Cas A. The amplitudes and phases of each interferometer spacing were calibrated by measurements of the point sources 3C 147 and 3C 380, typically at the beginning and end of each 12 hour observation. The assumed flux densities (see Table 1) are based on the data of Baars et al. (1977).

All 128 channel maps were inspected by eye using the display facilities available at DRAO. Those channel maps that show no H I emission were added up to construct a continuum map, which in turn was subtracted from all channel maps. Thus, the resulting maps contain only information on the H I emission. These maps will be referred to as line channel maps. Subsequently, all images were corrected for the response of the primary beam of the 9 m paraboloids modeled as a circular Gaussian function of 103′ FWHM. Further data processing was performed using the AIPS package. The conversion factor between brightness temperature and flux/beam is 0.02912 K (mJy beam^{-1})$^{-1}$.

The H I maps from the ST were deficient in information corresponding to interferometer baselines less than 13 m.

TABLE 1
OBSERVATIONAL PARAMETERS OF THE DRAO OBSERVATIONS

Parameter	Value
Right ascension of field center............	$20^{h}20^{m}28\overset{s}{.}0$ (J2000.0)
Declination of field center	$+43°51′14\overset{''}{.}0$ (J2000.0)
Observation dates..........................	1993 Jan
Total observing time	12×12 hr
21 cm calibration sources	3C 147 (22.0 Jy)
	3C 380 (14.2 Jy)
	S7 (100 K)
FWHM of synthesized beam	$1′59\overset{''}{.}58$ EW
	$2′54\overset{''}{.}58$ NS
Position angle of synthesized beam	$89°731$
FWHM of primary beam	$1°7$
Semiminor axis of first grating ring......	$2°8$
System Temperature T_{sys}.................	65 K
Continuum bandwidth	20 MHz
Spectrometer bandwidth	1 MHz
Number of channels	128
Velocity spacing...........................	1.65 km s^{-1}
Velocity resolution........................	2.64 km s^{-1}
Central velocity	-50 km s^{-1}
Clean continuum (rms noise)	~ 5 mJy beam^{-1}
Line channels (rms noise)	0.63 K (in T_b)

Separately H I observations of a 4° region centered on WR 140 were made with the DRAO 26 m paraboloid. These maps, containing information on the extended emission were calibrated with the standard region S7 (Williams 1973), spatially filtered and added to the synthesis maps following the procedure outlined by van der Werf & Higgs (1990).

As mentioned before, the same field observed for the H I line emission was simultaneously observed with the DRAO synthesis telescope in the continuum band adjacent to the 21 cm line. A total bandwidth of 20 MHz centered around the 21 cm line, with a notch filter removing the line contribution, was used in these observations. The 1420 MHz continuum map was made in the usual fashion by transforming calibrated, gridded visibilities, and CLEANed by a program employing the Clark algorithm (Clark 1980). The synthesized beamwidth (EW × NS) of the continuum map is $0\overset{''}{.}98 \times 1\overset{''}{.}41$, with the major axis along the position angle $1°3$. Later on the map was polar diagram corrected for the 103′ FWHM Gaussian response of the individual 9 m paraboloids. Short spacings were added up using standard procedures at DRAO.

3. OBSERVATIONAL RESULTS

3.1. Continuum Observations at $\lambda \sim 21$ cm

In Figure 1 the resultant radio continuum map toward WR 140 is shown. The position of the WR star is marked by a cross. This map shows the presence of pointlike sources, most of them likely to be extragalactic in origin, and extended emission. Within a circular region of radius $\sim 19′$, centered at the WR star position, the map is almost devoid of continuum emission above a 3 σ level, except for a pointlike source located $\sim 14\overset{'}{.}6$ arcmin to the northeast of HD 193793. The strongest extended emission is concentrated to the south and east of WR 140.

3.2. Neutral Hydrogen Line

Along $l \sim 81°$, the Galactic neutral hydrogen emission spans the velocity range $+30$ to -120 km s^{-1}. For the sake of presentation, a constant background corresponding to its mean brightness temperature was subtracted from each individual line channel map. The mean subtracted spectrum is shown in Figure 2. The main H I features arising from the general Galactic structure can be recognized. Unless otherwise stated, radial velocities in this paper will always be referred to the LSR.

To increase the signal to noise ratio (S/N), the original line channel maps were spatially convolved to yield a circular Gaussian beam response of FWHM = 3′. Thus, the final rms noise level, in brightness temperature units, in a single line channel map is $\Delta T_{rms} \sim 0.63$ K.

In order to proceed to the analysis of the H I data, a sample of 12 line channel maps, not shown here, was constructed. They covered the velocity range where the main H I features due to normal Galactic H I emission are present (see Fig. 2). Each map was the result of an average of five individual line maps (~ 8.25 km s^{-1}). Every map was searched for evidence revealing a possible interaction between the WR star and its surrounding ISM. To help us to distinguish between H I minima possibly associated with HD 193793 from those arising from the normal structuring of the ISM, the following criteria were adopted. (1) The WR star should appear projected onto, or close to, a region of
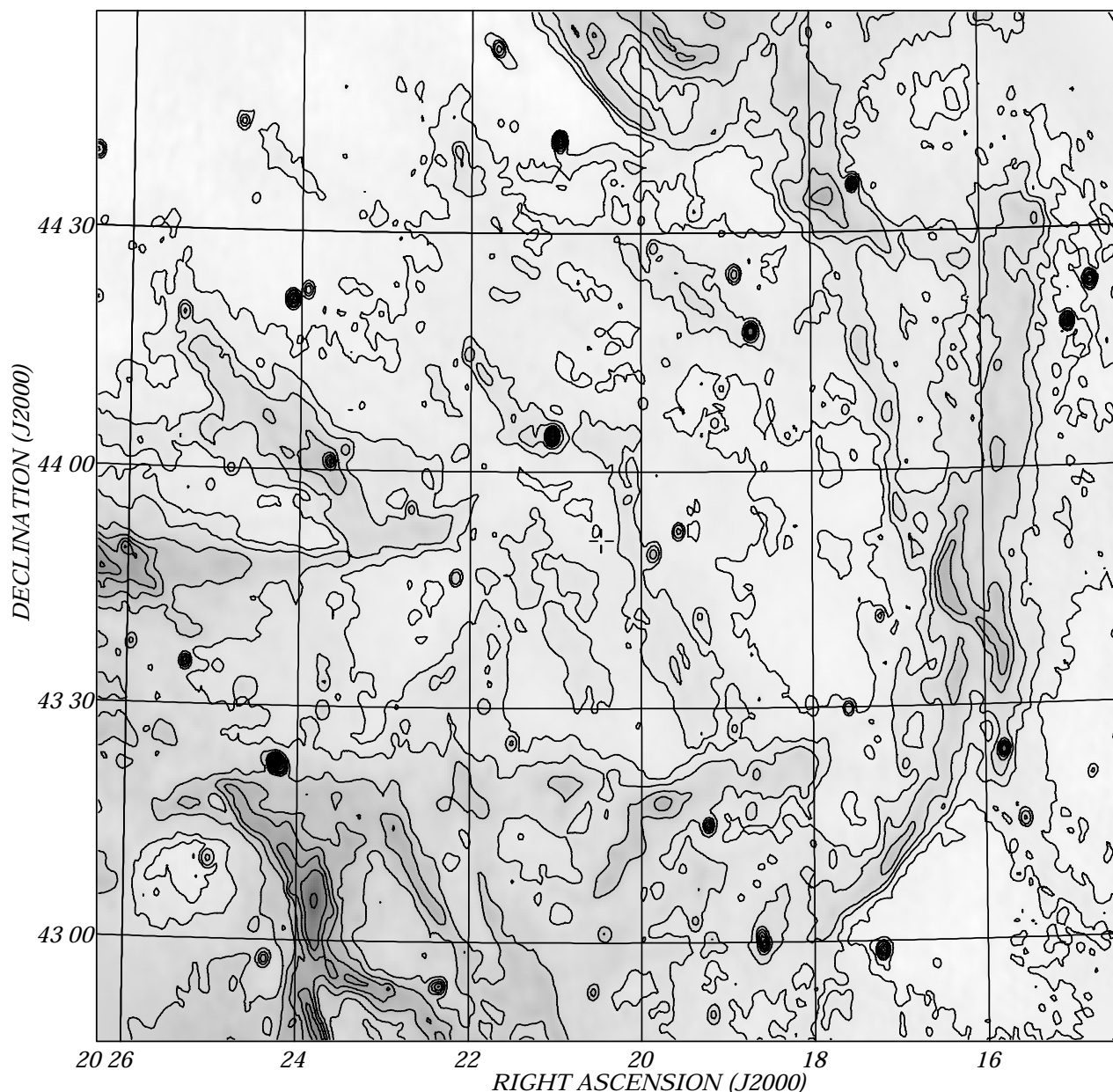
Fig. 1.—1420 MHz continuum radio emission in a 2° field centered on HD 193793. Short spacings have been added to this map. The stellar position is marked by a cross. The gray scale goes from 7 K (*light gray*) to 45 K (*dark gray*). Contour lines are shown from 9 to 11 K in steps of 1 K, then from 11 to 21 K in steps of 2 K, and from there upward the contour spacing is 5 K.

depressed H I emissivity. (2) The region mentioned above should remain observable throughout a significant number of *individual and consecutive* line channel maps. In our case we have set this number to five. (3) The kinematical distance derived from the mean radial velocity of the H I minimum should not be in great conflict with the accepted distance range for WR 140, namely, 0.8 to 1.45 kpc.

In the case of WR 140 the last criterion has a low weight, for along the Galactic longitude $l \sim 81°$ the velocity gradient is small, about 4.5 km s^{-1} kpc^{-1}, making the task of determining a "reliable" kinematical distance a particularly difficult one. In addition, one should bear in mind that significant noncircular motions are known to exist in this part of the Galaxy.

Among those twelve maps, only the one at -10.42 km s^{-1} shows a highly peculiar H I distribution. There the WR star is seen projected onto a well-defined minimum of the hydrogen gas emissivity. This feature is not observed in either adjacent map. In the velocity range covered by the H I emission, there is no other minimum in the hydrogen distribution having a reasonable morphological coincidence with the position of WR 140. No significant H I emission is detected outside the velocity range -125 to $+35$ km s^{-1}.

In Figure 3 eight individual line channel maps, covering the velocity range -5.48 km s^{-1} to -17.02 km s^{-1}, are displayed. Every map covers a circular region having a radius of 1° and is centered on the optical position of the
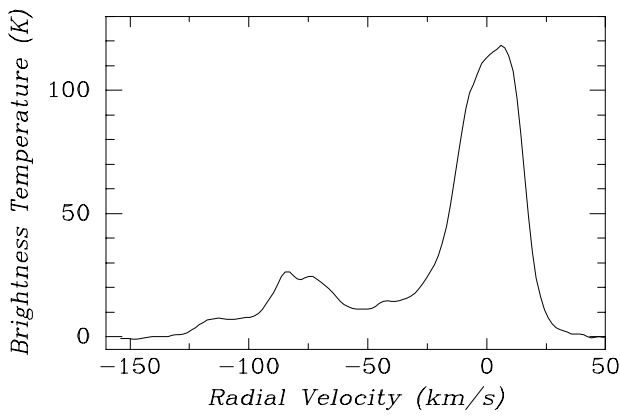
FIG. 2.—Spectrum that was subtracted from the H I maps for presentation. This spectrum is essentially that which would be observed by a 9 m dish telescope in the direction of WR 140.

WR star. In these maps the complex and rapidly changing appearance of the neutral gas distribution is evident.

4. DISCUSSION

4.1. *The Interaction of WR 140 with the ISM*

As mentioned in § 1, a H I cavity believed to be physically linked to WR 140 was detected by Arnal (1992) in the velocity range -20 to -7 km s^{-1}. However, the angular resolution of the Effelsberg observations, HPBW = 9′, precluded a detailed study of its spatial properties. Using the DRAO data, a much better characterization of both the spatial structure and the velocity field of the H I minimum can be made. Based on Figure 3, channel maps from -8.8 to -15.4 km s^{-1} were used to produce the mean H I brightness distribution map shown in Figure 4. The mean radial velocity of this map is -12.1 km s^{-1}. There, within the *main* H I minimum, two regions of lower H I emissivity are noticeable. The low H I emissivity region is clearly visible in the maps ranging from -8.78 down to -17.02 km s^{-1} (see Fig. 3). This velocity range is likely to
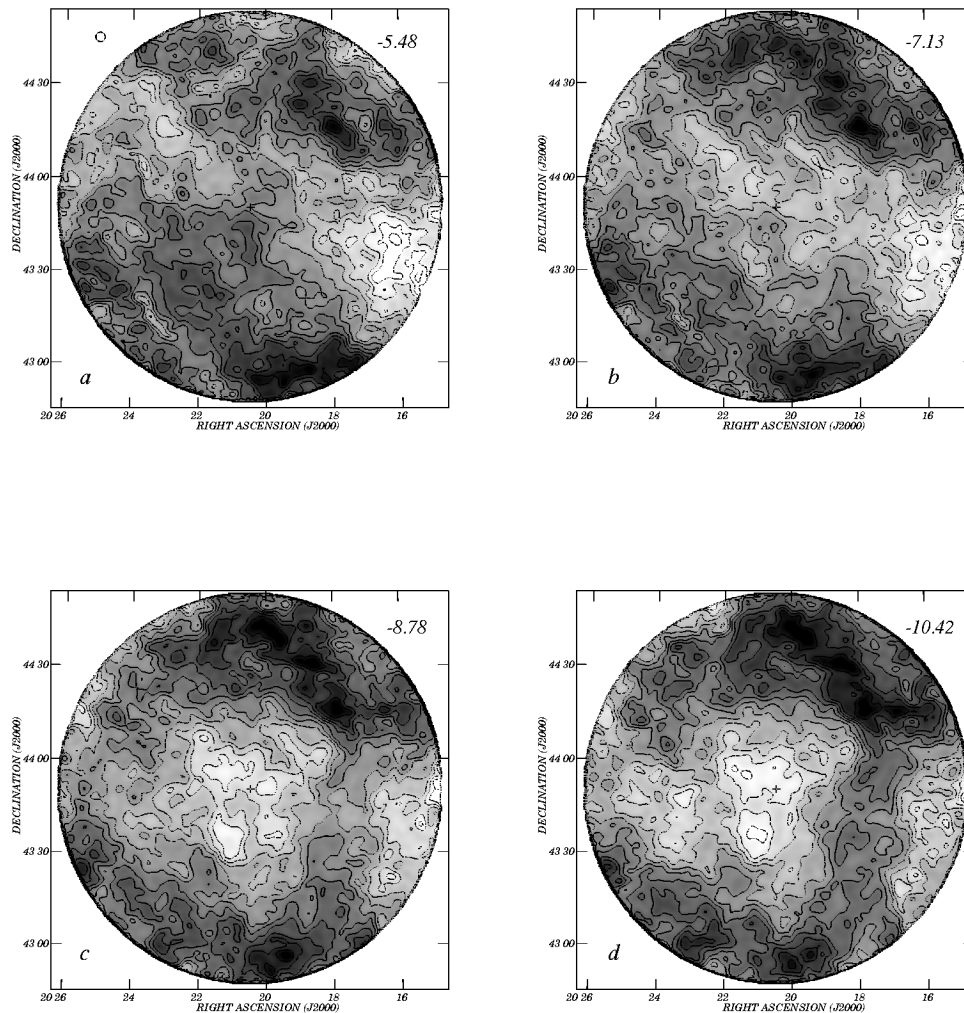

FIG. 3.—Mosaic of eight right ascension-declination H I mean brightness temperature maps obtained from the DRAO-ST data set for selected velocity ranges within the velocity interval -5.48 to -17.02 km s^{-1}. The central LSR velocity of each map is indicated at the top right corner. The open circle on the upper left corner of the first line map shows the DRAO beam (HPBW = 3′). Brightness temperature contours are given from -25 to $+30$ K in steps of 5 K (~ 8 σ). The gray-scale representation of these maps goes from light gray (-20 K) to dark gray ($+30$ K). All quoted temperatures are relative to the average brightness temperature at the corresponding velocity (see Fig. 1).
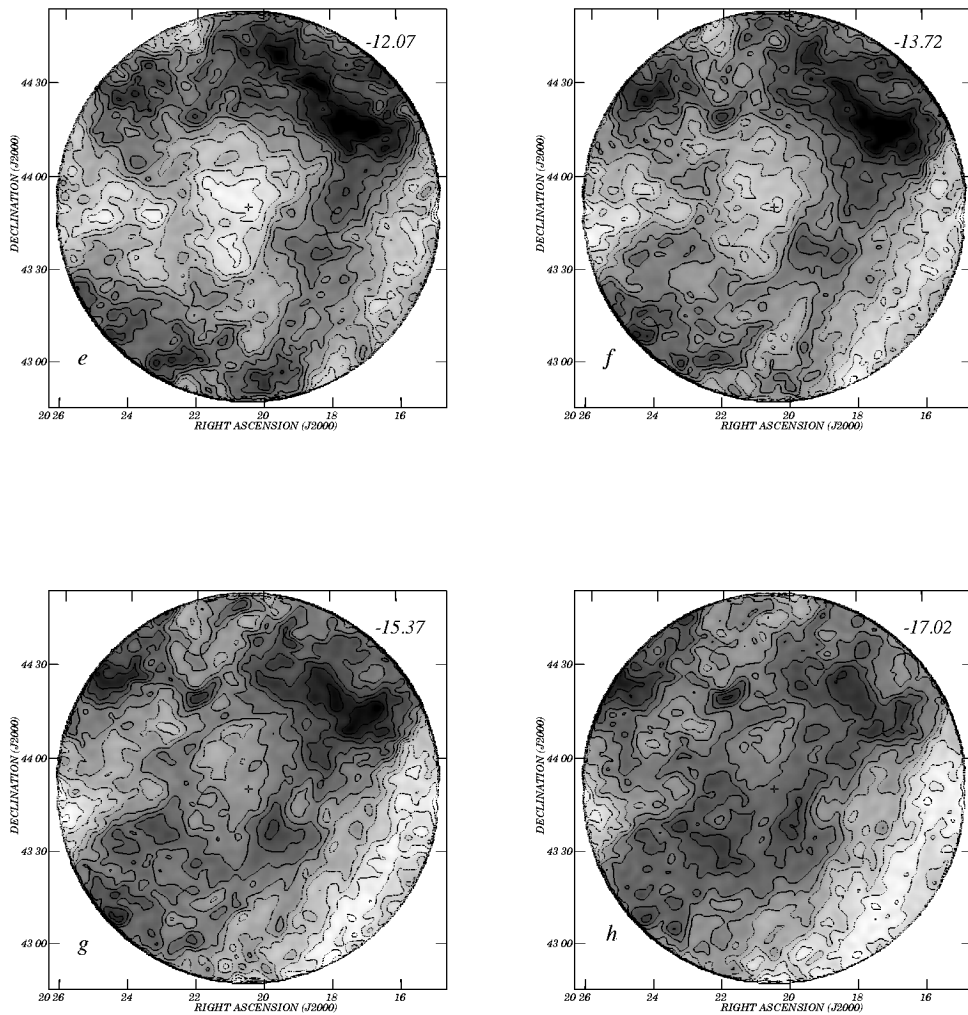
FIG. 3.—*Continued*

be a lower limit, for an H I minimum can also be recognized at channel maps having slightly higher (-7.13 km s^{-1}) and lower (-18.67 km s^{-1}) radial velocities. The criteria mentioned in § 3.2 for identifying a region of low H I emission gas as an interstellar bubble (IB) possibly related to a given WR star are met in the case of WR 140. However, the negative value of the radial velocity of the H I minimum may cast doubt on its physical relationship to WR 140. Adopting a mean radial velocity of -12 km s^{-1}, a rigorous application of the Galactic velocity field of Fich, Blitz, & Stark (1989) would place this cavity beyond the solar circle, at a distance of 5.0 ± 0.9 kpc. The large uncertainty reflects the small velocity gradient along the line of sight mentioned above and arises after allowance for noncircular motions of the order of ± 8 km s^{-1} is made. If this straightforward interpretation were correct, it would be impossible to link the H I minimum and WR 140 physically, for their distances would be too different. However, based on the kinematics exhibited by young open clusters having a Galactic longitude similar to that of WR 140, a negative radial velocity does not necessarily imply a location beyond the solar circle. Hron (1987) lists three open clusters (see his Table 1a) in the Galactic longitude range $75° \le l \le 79°$ that have mean radial velocities in the range from -13 to -4 km s^{-1}, even though their distances fall between 1.02 and 1.67 kpc. Hron claims that these clusters have both radial velocities

and distances accurate to 4 km s^{-1} and 20%, respectively. The Galactic velocity field of Fich et al. (1989) would place these clusters at a distance of ~ 5.4 kpc. Based on the above and bearing in mind that a WR star is expected to create an IB in its surrounding ISM, and since throughout the entire H I data cube we could not pinpoint another region of low neutral hydrogen emissivity close enough to WR 140, we believe that the H I cavity centered at -12 km s^{-1} is an IB created by the WR + O4-5 binary system during its evolution. Henceforth we refer to this H I minimum as to the *main* H I *minimum* (or *main minimum*, for short).

4.2. *Parameters of the Main Minimum*

The inner region of Figure 4 is shown at higher scale in Figure 5. It shows that the cavity is not spherical, but neither is it as elongated as the H I minima related to either WR 6 (Arnal & Cappa 1996) or WR 3 (Arnal & Roger 1997). As in Paper I, in order to derive a few parameters that may help us to define quantitatively the shape of the minimum, we have adopted as its outer border the highest-T close contour line defining the minimum. This level, denoted as T_{z1}, is -8 K for the main minimum. The properties of the *main* minimum are given in Table 2. Linear dimensions, mass, and volume density are derived assuming a distance of 1 kpc. Since the cavity parameters are somewhat dependent on the selected reference level, the values
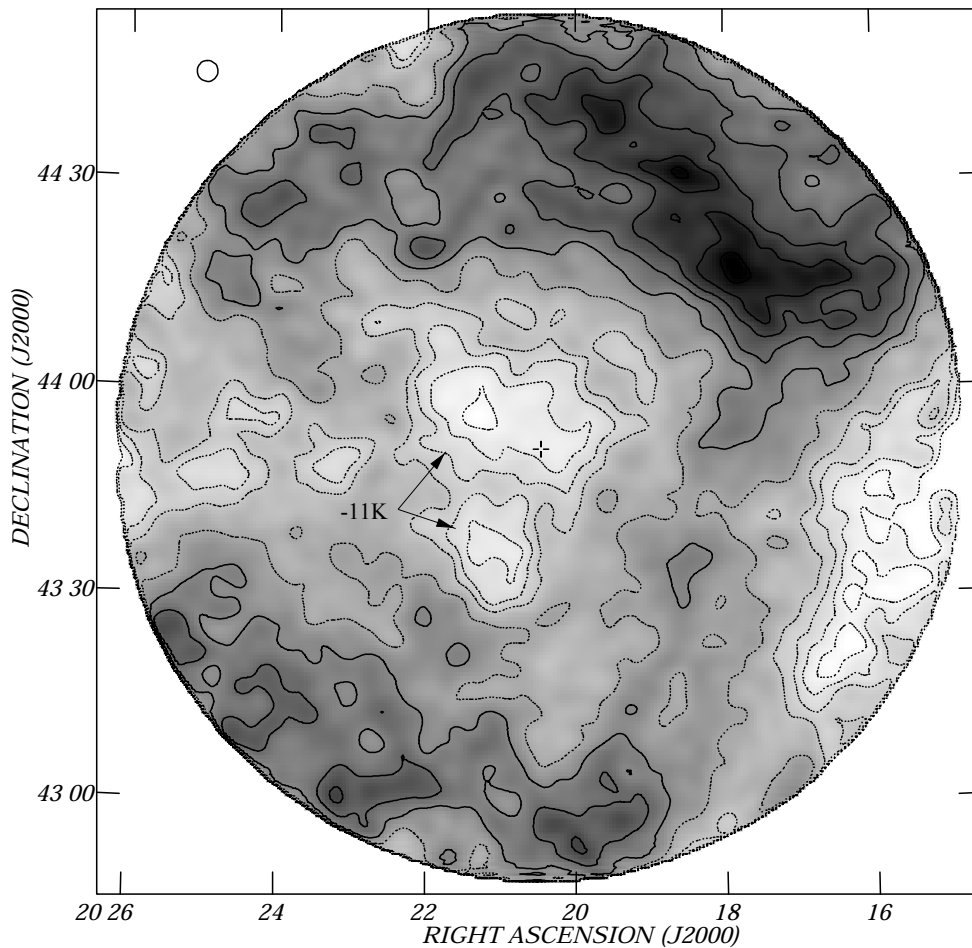
Fig. 4.—Gray-scale representation of the mean H I brightness temperature distribution toward WR 140. The angular resolution of this map is 3′ and the radial velocity covers the range from −7.1 to −15.4 km s^{-1}. Contour lines from −17 to −8 K are in steps of 3 K, and from −2 to 28 K are in steps of 6 K. The −11 K contour line is labeled. The position of the WR star is indicated by a cross. Notice that the WR star is seen projected toward a well-defined minimum of the overall neutral hydrogen emissivity. This minimum is surrounding by a patchy ridge of high H I emission.

quoted in Table 2 are a mean of measurements obtained at three different reference levels, namely, −8 ± 1 K. The H I minimum shown in Figure 5 stretches along the north-south direction. It major axis, d_M, is defined at a position angle of ∼165° (measured from north counterclockwise). Because of projection effects, d_M is likely to be a lower limit. The minimum extent perpendicular to d_M varies between ∼9.5 and ∼2.8 pc at the region connecting the two inner minima. Because of the geometry of the minimum related to WR 140, we have estimated a *mean* minor axis by setting the

TABLE 2

PROPERTIES OF THE MAIN H I MINIMUM

Parameter	Value
Geometric center, (α, δ) (J2000.0)	∼(20^h21^m0, +43°48′1)
Major axis, d_M (pc)[a]	11.5 ± 1.6
Mean minor axis, d_m (pc)[a]	8.4 ± 1.0
Axial ratio, C_{ax}	≥1.4 ± 0.4
Offset parameter, C_{off}	0.7 ± 0.2
Systemic velocity, V_{sys} (km s^{-1})	Approx. −12
Velocity extent Δv (km s^{-1})	≥11
Missing H I mass, $M_{H I}^{miss}$ ($M_\odot$)[a]	≥54
Missing H I density, $n_{H I}^{miss}$ (cm^{-3})[a]	≥0.7
Emission mass, $M_{H I}^{em}$ ($M_\odot$)[a]	∼1300

[a] Assuming a distance of 1.0 kpc.

measured area within the −8 K contour line equal to that of an ellipse of major axis d_M (measured) and minor axis d_m (derived). We define the midpoint of the major axis as the symmetry center (SC) of the H I minimum, as approximated by an ellipsoid.

As in Paper I, we define the axial ratio of the H I cavity, C_{ax} as the ratio of the major and minor axes, d_M/d_m, and an offset parameter, C_{off}, as the ratio of the projected distance of the WR star from the SC of the minimum to the minor axis, d_m. Owing to projection effects, both C_{ax} and C_{off} are likely to be lower limits.

We would like to stress that the velocity extent quoted in Table 2 corresponds to the velocity range where the H I depression remains detectable from an observational view-point. It should not be misinterpreted as an *expansion* velocity, for a geometrical model is needed to go from one to the other. Very likely, the velocity extent is probably a lower limit to the real velocity extent of the H I void, because "extreme"-velocity gas associated with the IB and set in motion by the WR star could be missed, owing to confusion effects. The systemic radial velocity, V_{sys}, represents the central value of the velocity range covered by the H I deficiency.

The missing H I mass, $M_{H I}^{miss}$, has been calculated for the H I minimum within the −8 K contour. Under the assumption that the H I gas is optically thin, the missing neutral
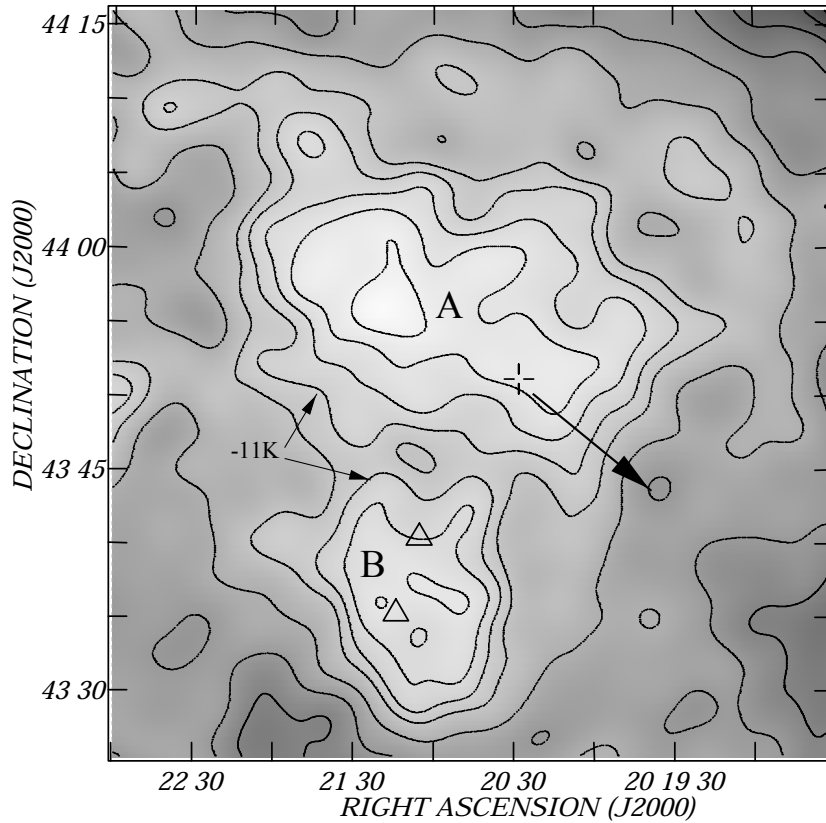
FIG. 5.—Close-up of the neutral hydrogen distribution observed in the neighborhood of WR 140. The figure covers a square region of 51' on the side. The position of the WR star is marked by a cross. The arrow indicates the proper motion direction of WR 140. The open triangles indicate the position of the stellar objects seen in projection against Object B (see § 5). Regions of low hydrogen emissivity are indicated by a light gray shading. Contour lines drawn from -17 to -9 K are in steps of 2 K ($\sim 8\ \sigma$); and from -5 to $+15$ K are in steps of 4 K ($\sim 16\ \sigma$). The -11 K contour is labeled. Notice the two well-developed inner minima within the main H I cavity.

hydrogen mass of a feature located at a distance d that covers a solid angle $\Omega_{\mathrm{H\,I}}$, whose mean brightness temperature over a velocity interval Δv is $\langle\Delta T\rangle$, is given by

$$M_{\mathrm{H\,I}}^{\mathrm{miss}} \simeq 0.014 d^2 \langle\Delta T\rangle \Delta v \Omega_{\mathrm{H\,I}}\ (M_\odot)\,, \qquad (1)$$

where $\langle\Delta T\rangle$, Δv, $\Omega_{\mathrm{H\,I}}$ and d are given in units of kelvins, kilometers per second, steradians, and parsecs, respectively. The mean brightness temperature $\langle\Delta T\rangle$ is defined as $|\langle T_{\mathrm{hole}}\rangle - T_{\mathrm{zl}}|$, where T_{zl} corresponds to the temperature of the contour level defining the outer border of the H I minimum and T_{hole} refers to the *mean* brightness temperature within that contour, $T_{\mathrm{hole}} = -11.9$ K. The missing H I mass represents the *minimum amount* of H I mass needed to "fill in" the observed H I minimum up to the -8 K contour. Since the H I minimum is detected *by contrast* with the surrounding H I emission, an alternative estimate of the missing mass is derived from a calculation of the H I mass needed to make the H I minimum *undetectable with respect to its average surrounding* neutral hydrogen emission. This mass is denoted as $M_{\mathrm{H\,I}}^{\mathrm{und}}$ and is given by

$$M_{\mathrm{H\,I}}^{\mathrm{und}} \sim M_{\mathrm{H\,I}}^{\mathrm{miss}} \left(1.0 + \frac{\langle\Delta T_{\mathrm{und}}\rangle}{\langle\Delta T\rangle}\right), \qquad (2)$$

where $\langle\Delta T_{\mathrm{und}}\rangle$ ($\equiv T_{\mathrm{sur}} - T_{\mathrm{zl}}$) is the mean brightness temperature excess of the surrounding emission. The other variables have the same meaning as before. Though it depends on the H I density prevailing in the neighborhood of the WR star (and its progenitor) at the time when they started

blowing away the surrounding gas, $M_{\mathrm{H\,I}}^{\mathrm{und}}$ very probably represents an upper limit to the missing H I mass. Using in Figure 3 those areas having a brightness temperature higher than -8 ± 1 K, a mean brightness temperature emission of $T_{\mathrm{sur}} \sim 3.1$ K was found. Using equation (2), this implies that the total amount of H I gas needed to render the H I minimum undetectable with respect to its surroundings is $\sim 208\ M_\odot$.

The missing H I density is obtained as the missing H I mass, $M_{\mathrm{H\,I}}^{\mathrm{miss}}$, divided by the volume of the H I minimum, assumed to be an ellipsoid with major axis, d_M, and both other axes equal to d_m:

$$n_{\mathrm{H\,I}}^{\mathrm{miss}} \simeq 79.2\ \frac{M_{\mathrm{H\,I}}^{\mathrm{miss}}}{d_M\, d_m^2}\ (\mathrm{cm}^{-3})\,, \qquad (3)$$

where $M_{\mathrm{H\,I}}^{\mathrm{miss}}$ is given in solar masses, and d_M and d_m in parsecs. Like $M_{\mathrm{H\,I}}^{\mathrm{miss}}$, $n_{\mathrm{H\,I}}^{\mathrm{miss}}$ is probably a lower limit to the ISM volume number density before a bubble was blown by the star.

The H I mass of the *surrounding* emission ($M_{\mathrm{H\,I}}^{\mathrm{em}}$) can also be derived from equation (1), when $\langle\Delta T\rangle$ is replaced by $\langle\Delta T_{\mathrm{und}}\rangle$ and $\Omega_{\mathrm{H\,I}}$ by Ω_{em}. The latter refers to the solid angle subtended by those pixels having a brightness temperature equal to or higher than -8 K.

5. THE MAIN CAVITY AND ITS INNER STRUCTURE

Interior to the contour line defining the border of the H I minimum (Fig. 5), there are two H I minima. Adopting for

them $T_{z1} = -11$ K and using a similar procedure to that outlined for the main minimum, their physical properties were derived. They are given in Table 3. The northern minimum will be referred to as object "A," and the southern one as object "B." As mentioned in Paper I, multiple minima may result from the presence of stellar objects unevenly distributed over the area delimited by the main cavity. Since WR 140 is not known to be a member of either an open cluster or an OB association (Lundström & Stenholm 1984), using the SIMBAD database, a thorough search was conducted for stellar objects other than WR 140 within the solid angle of the main cavity. The results are given in Table 4. Only the WR star HD 193793 is seen in projection onto object A. Two stars, marked in Figure 5 as open triangles, are found to fall inside the defining contour level of object B. Of these, HD 193926 is a double star with a parallax of $\pi = 4.57 \pm 0.74$ mas (ESA 1997). Thus, it is a foreground object. The other object, SAO 49504 is a triple stellar system; it has no measured parallax in the *Hipparcos* main catalog, and its principal component has a visual magnitude of 9^m0. Components B and C have a visual magnitude of 9.2 and 10.7 mag, respectively, and are located $0\farcs2$ and $2\farcs0$ away from the main component (Dommanget & Nys 1995). The spectral type provided by SIMBAD, namely, A2, very likely represents the *combined* spectral type of components A and B. If this system were located at a distance of ~ 1 kpc, with a similar reddening to that of WR 140, namely, $A_v = 2.5$ mag, its absolute magnitude would be -3.3 mag. Bearing in mind that the adopted absorption is poorly known and that we may be dealing with the combined spectral type of at least two stars, only if the later type resembles that of a bright giant (luminosity class II) the triple system may be physically linked to object B.

Based on the above, WR 140 and its companion are the only stellar objects capable of having created object A, while a key role of SAO 49504 in the formation of object B

cannot be entirely ruled out for the time being. Arnal (1992) has argued that WR stars are often associated with double H I cavities in which the star usually appears off-center. For the sake of clarity, it is worth mentioning that an H I cavity is said to possess a dual-minimum geometry when *both* H I minima could have been originated by *the same* stellar object. Though the H I cavity detected around WR 140 shares most of the morphological characteristics of the dual-minimum H I cavities previously observed, the possibility that object B could have been formed by SAO 49504 cast some doubt on such a straightforward classification. Keeping the above in mind, the main H I cavity would be classified as one *possibly* showing a dual-minimum geometry.

5.1. *Shape of the Cavity*

In the idealized hydrodynamics theory of IB, aspherical shapes can result when (1) the star moves with a *high spatial velocity* with respect to its surrounding medium, (2) the ambient ISM density is *not* uniform, and (3) the stellar wind arising from a region close to the stellar object is *not* isotropic. In this last case, the stellar wind itself may by aspherical, or else the stellar wind is intrinsically isotropic but encounters, close to the star, some sort of obstacle that blocks or deflects it. In the presence of an ISM magnetic field an ambient shock will expand faster along the field direction, and the resulting IB will be elongated (Stone & Norman 1992).

HD 193793 has a proper motion of $\mu_\alpha = -5.36 \pm 0.58$ mas and $\mu_\delta = -2.37 \pm 0.49$ mas (ESA 1997). This implies a total proper motion of $\mu = 5\farcs86 \pm 0.57$ mas, which at 1 kpc translates to a tangential velocity of $V_t = 28 \pm 3$ km s^{-1}. The position angle of the proper-motion vector (see Fig. 5) is $66° \pm 5°$ (measured from north counterclockwise), close to the position angle of the major axis of object A. The shape of object A could result from the spatial motion of WR 140 (Weaver et al. 1977).

If the star had *always* been moving with such velocity, it would have displaced some $\sim 0\fdg8$ (or ~ 28 pc) within a WR phase lifetime of about 5×10^5 yr (Maeder & Meynet 1994). This angular distance is larger than the major axis of the H I main minimum by a factor of about 3. Thus, if the star has *always* been in this state of motion, then the observed coincidence of the H I cavity and WR 140 is accidental. On the other hand, if WR 140 *is* the cause of the H I cavity, then the binary system must have acquired its spatial velocity recently. Based on the evidence presented so far, genuine association appears likely.

If we suppose that the stellar system was originally close to the symmetry center (SC) of object A, the time required to reach its present position would be about 1.3×10^5 yr.

TABLE 3

PARAMETERS OF THE INNER H I MINIMA

Parameter	Object A	Object B
R.A. center (α) (J2000.0)	$\sim 20^h21^m0$	$\sim 20^h21^m2$
Decl. center (δ) (J2000.0)	$\sim 43°55\farcm72$	$\sim 43°36\farcm23$
Major axis, d_{Mh} (pc)[a]	7.7 ± 0.4	3.8 ± 0.5
Position angle, d_{Mh} (deg)	~ 64	~ 3
Axial ratio, C_{ax}	1.8 ± 0.3	1.4 ± 0.4
Offset ratio, C_{off}	$\sim 0.6 \pm 0.2$	$\sim 1.9 \pm 0.4$
H I mass, M_{HI}^{miss} ($M_\odot$)[a]	≥ 11.2	≥ 2.3
H I density, n_{HI}^{miss} (cm^{-3}) [a]	≥ 0.8	≥ 0.8

[a] Assuming a distance of 1.0 kpc.

TABLE 4

STELLAR OBJECTS SEEN IN PROJECTION TOWARD THE MAIN H I CAVITY

Object	Sp. Type[a]	m_v (mag)	R.A.	Decl.	Remarks
HD 193793	WC7	6.89	20 20 27.97	+43 51 16.27	Binary, object A
SAO[b] 49504	A2	9.23	20 21 05.3	+43 40 30.7	Triple system, object B
HD 193926	A0	7.86	20 21 14.04	+43 35 21.5	Binary, object B

NOTE.—Units of right ascension are hours, minutes, and seconds, and units of declination are degrees, arcminutes, and arcseconds (J2000.0).

[a] Unless otherwise stated quoted as provided in SIMBAD.

[b] SAO = Smithsonian Astronomical Observatory star number.

This is a fraction of the time spent by a massive star in its WR phase (Maeder & Meynet 1994) and would indicate that something changed the velocity of the present binary system (e.g., the disruption of a hierarchical triple-star system; Kiselva 1996) that gave WR 140 and its companion their present velocity. The Wolf-Rayet star HD 191765 ($\equiv$ WR 134) exhibits a similar dynamical behavior (Gervais & St-Louis 1999).

6. AN INFRARED COUNTERPART

Of the IB studies in the H I line with high angular resolution, only a very small sample has a counterpart at other frequencies. Figure 6 shows a map of the emission at 100 μm. WR 140 is projected onto a region of low-infrared emission, surrounded by a ringlike feature of enhanced emission. The circumference drawn in Figure 6 corresponds to the *IRAS* shell reported by Marston (1996), and the position of WR 140 is marked by a cross.

Figure 6 also reveals a wealth of structure in the IR emission toward the interior of the shell. Figure 7 gives an overlay of the IRAS 100 μm emission and the H I distribution. Due to the relatively high Galactic latitude of WR 140, a line-of-sight coincidence between a minimum in the H I distribution and a similar minimum at infrared wavelengths is unlikely. The central location (with respect to the IR shell)

of the WR star also argues against a chance coincidence. Thus, we believe the IR shell and the H I minimum are both observational manifestations of the large energy input to the surrounding ISM by WR 140 and its companion. A similar conclusion was reached by Marston (1996). In the inner region, there are two IR minima separated by a thin ridge of enhanced IR emission. These minima are located at $(\alpha, \delta) = (20^h22^m36\overset{s}{.}6, +44°06'32'')$ and $(20^h19^m36\overset{s}{.}3, +43°49'26'')$ and will be referred to as IREM and IRWM, respectively. The WR star HD 193793 is seen projected onto the eastern border of IRWM, and most of object A in the H I map falls onto the ridge of enhanced IR emission that separates the IR minima.

What other evidence exists for *physically* linking the IR shell to WR 140? Since interstellar grains achieve their equilibrium temperature primarily by radiative processes (Whittet 1992), a dust temperature higher than the typical value derived for dust heated by the interstellar radiation field (ISRF) would also suggest physical association.

Using 60 and 100 μm HIRES *IRAS* images, the infrared shell was divided into six regions. Their IR fluxes, derived after removing a local emission background, are given in Table 5. The first column identifies the region, the second and third provide the centroid coordinates, the fourth its solid angle, the fifth and sixth the estimated flux density,
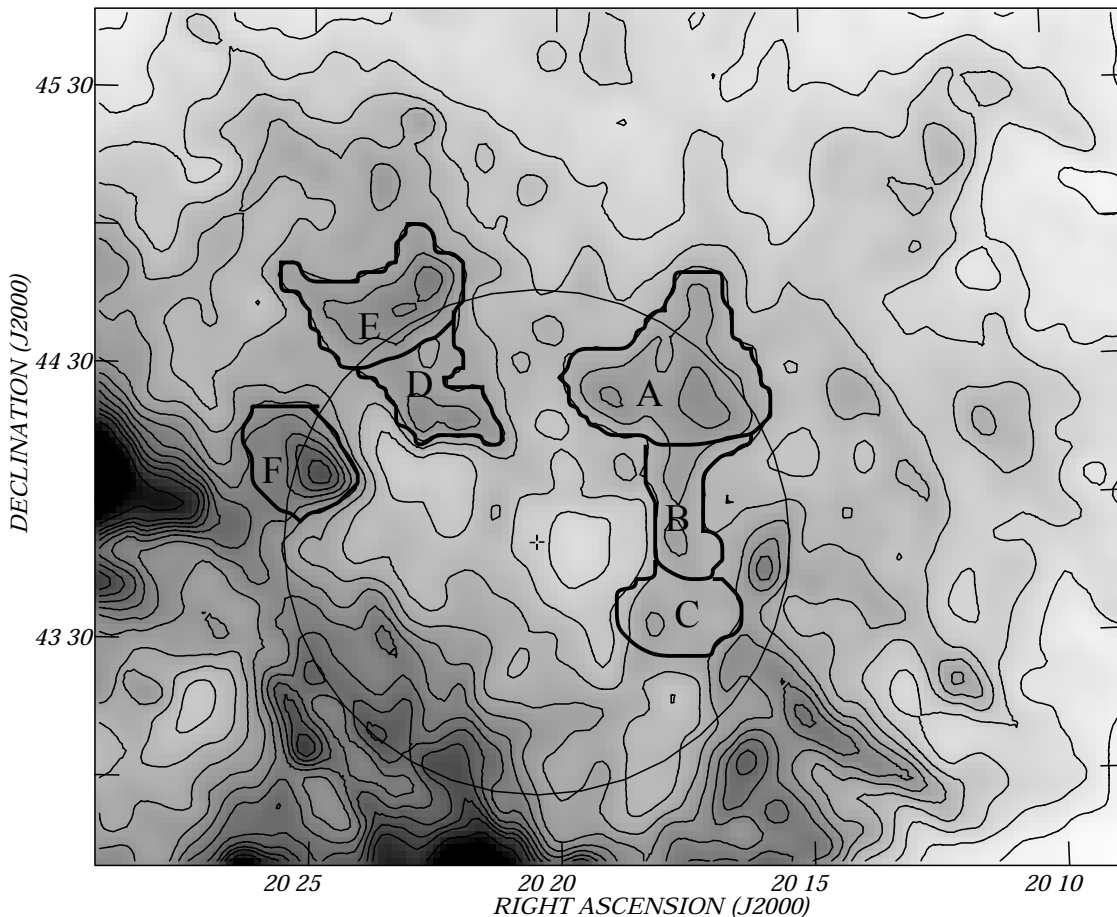

FIG. 6.—Infrared dust emission as traced by the IRAS 100 μm band toward WR 140. The minimum and maximum 100 μm IR emission in the field are 75 MJy sr^{-1} (*light gray shading*) and 500 MJy sr^{-1} (*dark gray representation*), respectively. The cross indicates the location of WR 140. Notice that WR 140 is seen projected onto a minimum of the IR distribution that is surrounded by a shell-like feature. The circumference marks the position of the IR-shell found by Marston (1996). The contour lines go from 100 to 400 MJy sr^{-1} in steps of 25 MJy sr^{-1}, and from 400 to 500 MJy sr^{-1} in steps of 50 MJy sr^{-1}. The location of the six regions used to derive the dust temperature given in Table 5 are shown by thick contour lines.
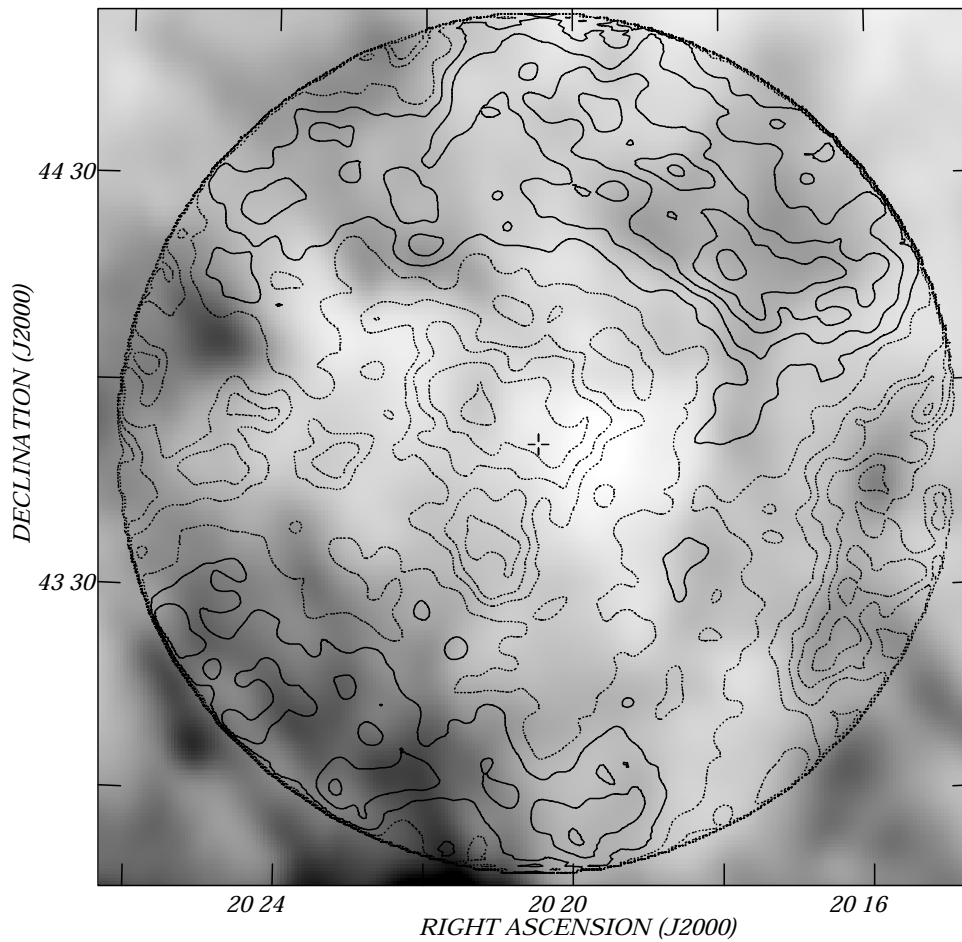
Fig. 7.—Overlay of the dust emission at 100 μm and the neutral gas brightness temperature in the H I 21 cm line. The infrared emission is depicted by gray shading, while the H I emission is shown by contour lines. The minimum and maximum 100 μm emission are ~ 77 MJy sr^{-1} (*light gray shading*) and ~ 600 MJy sr^{-1} (*dark gray shading*), respectively. The contour lines are those shown in Fig. 4. The cross indicates the location of WR 140. The outer circular contours delineate the 103′ field of view of our DRAO H I observations.

and the last provides the mean dust temperature, T_d. This temperature was derived by fitting to the data a modified Planck function of the form $v^m \times B_v(T_d)$. The frequency dependence of the dust absorption cross-section is given by the factor v^m. The value adopted for m is 2. The errors quoted for T_d are derived on the assumption that the IR fluxes at 60 and 100 μm are accurate to 21% and 32%, respectively (Fich & Terebey, 1996). The derived dust temperatures are systematically higher in regions of the IR shell

to the west of WR 140. The mean dust temperature for regions A, B, and C is $T_d = 31.2 \pm 2.7$ K, compared with $T_d = 27.9 \pm 1.7$ K, for regions D, E, and F. Because of possible confusion effects with unrelated emission, we include in this analysis only those parts of the IR shell that on geometrical grounds alone are clearly recognizable as belonging to the IR-emitting dust shell.

Another way of detecting heated dust is to look at the so-called IR-excess emission map (see van Buren, Noriega-

TABLE 5
MEASURED INFRARED FLUXES

Region	R.A.	Decl.	Ω (sr)	$S_{60\ \mu m}$ (Jy)	$S_{100\ \mu m}$ (Jy)	T_d (K)
A	20 17 30	+44 25 40	8.3×10^{-5}	1806	3884	29.5 ± 2.0
B	20 17 30	+43 54 40	2.7×10^{-5}	541	7587	34.3 ± 2.5
C	20 17 30	+43 32 40	9.7×10^{-5}	1632	3452	29.7 ± 2.0
D	20 22 15	+44 24 00	5.1×10^{-5}	747	2093	27.0 ± 1.7
E	20 23 20	+44 45 30	1.0×10^{-4}	752	2135	26.9 ± 1.7
F	20 25 15	+44 07 55	5.1×10^{-5}	829	1706	29.9 ± 2.1

NOTE.—Units of right ascension are hours, minutes, and seconds, and units of declination are degrees, arcminutes, and arcseconds (J2000.0).
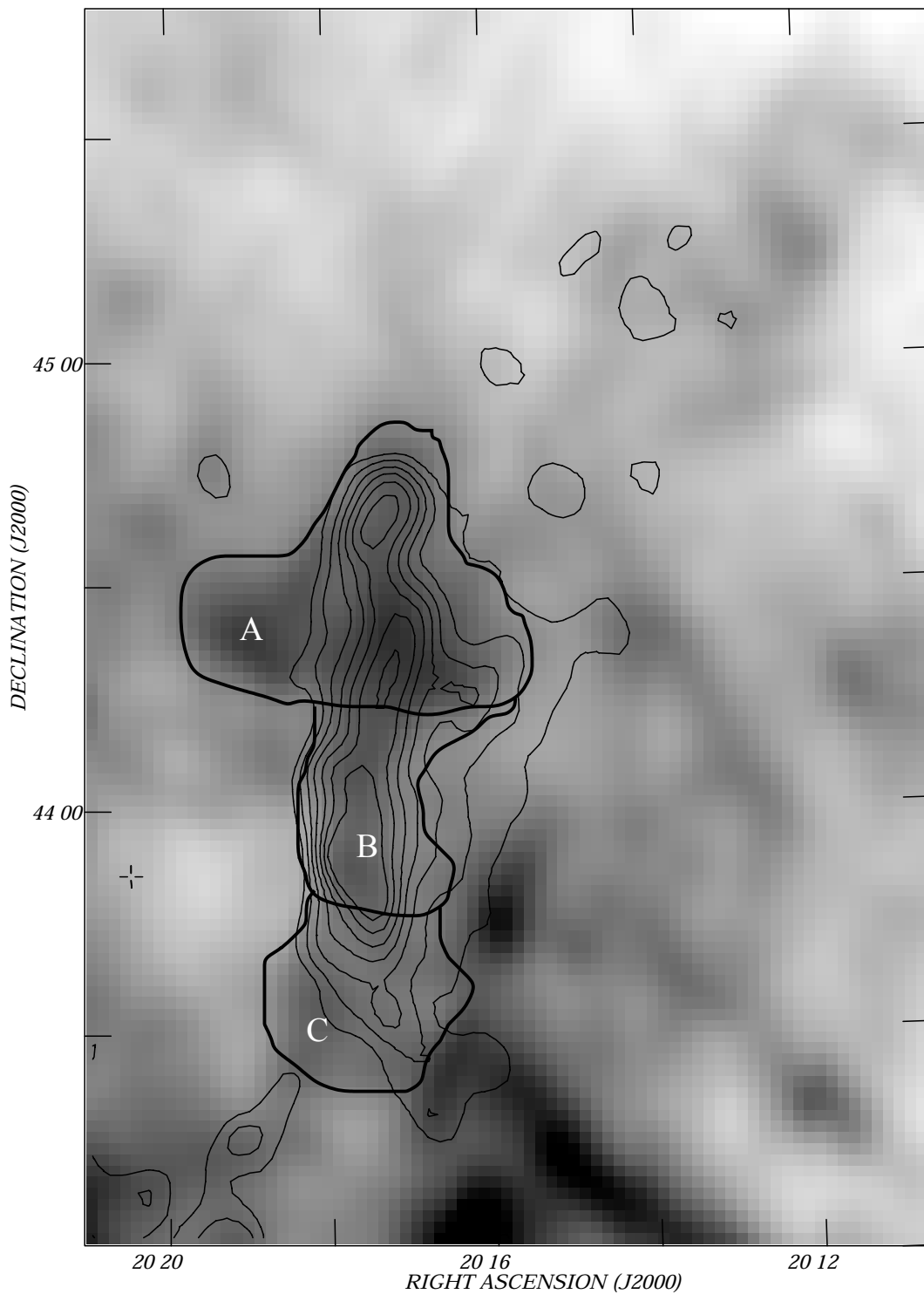
Fig. 8.—Overlay of the 100 μm *IRAS* map (*gray shading*) and the 60 μm excess emission. Only the western part of the large *IRAS* shell is displayed. The minimum and maximum 100 μm emission are $\sim$98 MJy sr^{-1} (*light gray*) and $\sim$335 MJy sr^{-1} (*dark gray*), respectively. The 60 μm infrared excess emission is given by thin solid lines. The lowest contour is 10 MJy sr^{-1}, and the contour step is 2.5 MJy sr^{-1}. The location of the infrared regions A, B, and C is given by thick solid lines. The position of WR 140 is marked by a cross.

Crespo, & Dgani 1995). Based on the original 60 and 100 μm *HIRES* maps, a 100 μm–based 60 μm IR-excess map was produced. The original maps were first smoothed to the same angular resolution (a circular beam 4′ was chosen). Afterward, a pixel-by-pixel scatter diagram of the 60 versus 100 μm pixel intensities within two control areas containing

only weak and diffuse emission was produced, and a straight line was fitted to the data. Relying on the fit parameters of the control areas and using the *IRAS* maps observed *toward* WR 140, the expected 60 μm background emission was computed and subtracted from the original map. This map shows only excess 60 μm IR emission and is

a good tracer of heated dust. A blowup of the western region of the IR shell shown in Figure 6 is shown in Figure 8. The original 100 μm map is shown as a gray shading, while the contour lines show the 60 μm IR-excess map. The area showing a noticeable excess of IR emission is coincident with regions labeled A, B, and C in Table 5.

According to van Buren & McCray (1988), the dust temperature of two regions whose dust grains are heated predominantly by the UV radiation field of a stellar source are related by

$$\frac{T_d^1}{T_d^2} = \left(\frac{r_2}{r_1}\right)^{1/3}, \tag{4}$$

where r_1 and r_2 are the distance of those regions from the stellar source, and T_d^1 and T_d^2 their corresponding dust temperatures. Adopting for T_d^1 and T_d^2 the mean dust temperatures for regions A, B, C ($T_d = 31.2$ K) and D, E, F ($T_d = 27.9$ K), from equation (2) we find $r_2/r_1 \sim 1.4$. Using the centroid coordinates for regions A to F given in Table 5 and the coordinates of WR 140, a mean projected angular distance ratio of $r_2/r_1 \sim 1.3$ is derived. Assuming that projection effects play a minor role, the mean projected angular distance ratio can be interpreted as a true distance ratio, providing extra support to the idea that the IR-emitting features may be dust heated by the radiation field of both the WR star and its O companion.

Though there is an overall spatial correlation between the *IRAS* shell and the H I shell that surrounds the main H I minimum (see Fig. 7), the distribution of the IR emission observed toward the inner area of the IR-shell has little resemblance to the distribution of the neutral gas, object B has no counterpart at IR wavelengths, and object A is projected on an IR distribution showing two minima. This dual-minimum IR appearance is mainly caused by the presence of a 22' long barlike IR feature (the bar from here onward), whose south end lies at $(\alpha, \delta) = (20^h21^m32\overset{s}{.}7, +43°47'02'')$.

If this bar were physically close to WR 140, it would be exposed to a copious rain of Lyman continuum photons that would both ionize its gaseous matter and heat its dust grains. From the *HIRES* images mentioned above, after removing a local infrared background, the infrared fluxes at 60 and 100μm are ~160 Jy and ~414 Jy, respectively. Assuming thermal emission and a grain emissivity varying as v^2, these fluxes imply a dust temperature of $T_d \simeq 28 \pm 2$ K. This is similar to the mean T_d obtained for regions D, E, and F, namely, $T_d \simeq 27.9 \pm 1.7$ K. Thus, very likely the small angular distance between the bar and WR 140 is a projection effect. An additional piece of evidence in this direction comes from the 1420 MHz continuum map, which shows no feature above a 3 σ level at the position of the bar. Based on these facts, we believe the dual-minimum IR appearance is caused by the projection of the bar onto an otherwise single IR minimum.

7. A RADIO CONTINUUM COUNTERPART?

In the continuum map (Fig. 1), there is an arc-shaped feature almost 1°5 long $\sim45'$ westward of WR 140. At first sight this feature shows a good morphological agreement with the western parts of both the *IRAS* and H I shells. However, a close examination shows that the feature falls onto the *outer* part of both shells. Therefore, it is unlikely that this emission originates in an ionized counterpart of the neutral gas shell that surrounds WR 140, for in that case the continuum feature should be *interior* to both shells.

8. CONCLUSIONS

In studying the ISM local to WR 140 by means of high angular resolution H I observations, the neutral gas matter distribution in that region was studied in great detail. Our main results can be summarized as follows.

1. A large ovoid H I minimum close to the optical position of the WR star HD 193793 was detected. This feature is surrounded by a clumpy shell of neutral gas. The void of H I, which has a linear size of 11.5 × 8.4 pc, remains detectable throughout the velocity range -7.13 to -18.67 km s^{-1}.

2. Inside the main H I minimum, two well-developed minima are easily noticeable. One of them, object A, has probably been formed as a consequence of the action of both the stellar radiation field and the high mass-loss rate of the binary system. If the composite spectrum of components A and B of SAO 49504 resembled that of a bright giant, this triple stellar system could have played a role in shaping object B. Otherwise, the star must be unrelated to this H I feature, and the main minimum could be added to the short list of Galactic WR stars related to H I minima displaying a dual-minimum geometry.

3. The major axis of object A lies along the stellar motion direction derived from the proper motions of HD193793. This suggests that both the elongated shape of this minimum and the off-center location of WR 140 with respect to object A stem from the spatial motion of WR 140.

4. The systemic velocity of the H I minimum, -12 km s^{-1}, argued to be at the WR distance of about 1 kpc, implies that there are important peculiar motions in the ISM along $l = 81°$ at approximately 1 kpc from the Sun.

5. The apparent reality of the physical link between the H I cavity and WR 140 suggests that the binary system was set in motion as a whole some 1.3×10^5 yr ago. A process such as the disruption of a hierarchical triple-star system could result in the observed spatial velocity deduced for the binary system.

6. The clumpy shell of H I surrounding the *main* minimum has a counterpart at IR wavelengths. This implies a similar overall spatial distribution of the atomic gas (as revealed by the neutral hydrogen observations) and the dust particles (as traced by the IR emission). Of the small-scale structures toward the interior of both the IR and H I shells, only object A has a counterpart at IR wavelengths.

REFERENCES

Arnal, E. M. 1992, A&A, 254, 305
Arnal, E. M., & Cappa, C. E. 1996, MNRAS, 279, 788
Arnal, E. M., & Roger, R. S. 1997, MNRAS, 285, 253 (Paper I)
Baars, J. W. M., Genzel, R., Pauliny-Toth, I. I. K., & Witzel, A. 1977, A&A, 61, 99
Becker, R. H., & White, R. L. 1985, ApJ, 297, 649
Clark, B. G. 1980, A&A, 89, 377
Conti, P. S., & Vacca, W. D. 1990, AJ, 100, 431
Dommanget, J., & Nys, O. 1995, Bull. d'Inf. CDS, 46, 3
ESA. 1997, The Hipparcos and Tycho Catalogue (ESA SP-1200) (Noordwijk: ESA)
Fich, M., Blitz, L., & Stark A. A. 1989, ApJ, 342, 272
Fich, M., & Terebey, S. 1996, ApJ, 472, 624
Gervais, S., & St-Louis, N. 1999, AJ, 118, 2394
Hidayat, B., Supelli, K., & van der Hucht, K. A. 1982, in IAU Symp. 99, Wolf-Rayet Stars: Observations, Physics, and Evolution, ed. C. W. H. de Loore & A. J. Willis (Dordrecht: Reidel), 27
Hron, J. 1987, A&A, 176, 34
Kiselva, L. G. 1996, in IAU Symp. 174, Dynamical Evolution of Star Clusers—Confrontation of Theory and Observations, ed. P. Hut & J. Makino (Dordrecht: Kluwer), 233
Lamontagne, R., Moffat, A. F. J., & Seggewiss, W. 1984, ApJ, 277, 258
Lundström, I., & Stenholm, B. 1984, A&AS, 58, 163
Maeder, A., & Meynet, G. 1994, A&A, 287, 803
Marston, A. P. 1996, AJ, 112, 2828
Nugis, T., Crowther, P. A., & Willis, A. J. 1998, A&A, 333, 956

Roger, R. S., Costain, C. H., Lacey, J. D., Landecker, T. L., & Bowers, F. K. 1973, Proc. IEEE, 61, 1270
Skinner, S., Nagase, F., Koyama, K., Maeda, Y., & Tsuboi, Y. 1995, in IAU Symp. 163, Wolf-Rayet Stars: Binaries, Colliding Winds, Evolution, ed. K. A. van der Hucht & P. M. Williams (Dordrecht: Reidel), 471
Smith, L. F., Shara, M. M., & Moffat, A. F. J. 1990, ApJ, 358, 229
Stone, J. M., & Norman, M. L. 1992, ApJ, 389, 297
van Buren, D., & McCray, R. 1988, ApJ, 329, L93
van Buren, D., Noriega-Crespo, A., & Dgani, R. 1995, AJ, 110, 2914
van der Hucht, K. A. 1992, A&A Rev., 4, 123
van der Hucht, K. A., Hidayat, B., Admiranto, A. G., Supelli, K. R., & Doom, C. 1988, A&A, 199, 217
van der Werf, P. P., & Higgs, L. A. 1990, A&A, 235, 407
Veidt, B. G., Landecker, T. L., Vaneldik, J. F., Dewdney, P. E., & Routledge, D. 1985, Radio Sci., 20, 1118
Weaver, R., MacCray, R.,& Castor, J. 1977, ApJ, 218, 377
Whittet, D. C. B. 1992, Dust in the Galactic Environment (New York: Inst. Phys.)
Williams, D. R. W. 1973, A&AS, 8, 505
Williams, P. M., van der Hucht, K. A., Pollock, A. M. T., Florkowski, D. R., van der Woerd, H., & Wamsteker, W. M. 1990, MNRAS, 243, 662
Williams, P. M., van der Hucht, K. A., van der Woerd, H., Wamsteker, W. M., Geballe, T. R., Garmany, C. D., & Pollock, A. M. T. 1987, in Instabilities in Luminous Early-Type Stars, ed. H. J. G. L. M. Lamers & C. W. H. de Loore (Dordrecht: Reidel), 221